R.V. GĂDĂLEAN[1,2*], O.-D. JUCAN[3], H.F. CHICINAŞ[2,3], N. BÂLC[1], C.O. POPA[3]

ADDITIVE MANUFACTURING OF WC-Co BY INDIRECT SELECTIVE LASER SINTERING (SLS) USING HIGH BULK DENSITY POWDERS

Research in additive manufacturing of tungsten carbide-cobalt has intensified over the last few years due to the increasing need for products designed using topology optimisation and multiscale structures (lattice). These products result in complex shapes and contain inner structures that are challenging to produce through conventional techniques, thus involving high costs. The present work addresses this problem using a two-step approach to 3D print parts with complex shapes and internal structures by employing indirect selective laser sintering (SLS) and tungsten carbide-cobalt sintering. The paper takes further our research in this field [1] to improve the part density by using high bulk density tungsten carbide-cobalt powders. Mechanically mixing tungsten carbide-cobalt with the sacrificial binder, polyamide 12, results in a homogenous powder successfully used by the selective laser sintering process to produce green parts. By further processing, the green parts through a complete sintering cycle, an average final part density of 11.72 g/cm^3 representing more than 80% of the theoretical density is achieved.

Keywords: additive manufacturing; selective laser sintering; cemented carbide; polyamide 12

1. Introduction

Additive manufacturing (AM) represents the general term used for all technologies that fabricate parts through the addition of material [2]. The addition is executed layer by layer, starting with a computer-generated 3D CAD model, which is sliced into equal thickness layers. These layers are added on top of each other, thus creating a physical three dimensional part [2,3]. AM technologies' ability creates a direct connection between the virtual and physical world, enabling designers to tackle challenges with increased freedom regarding product design [4].

Since the invention of the first AM technology, stereolithography (SLA), in 1983 by Charles W. Hull [5], the AM industry has known a significant increase, reaching a $4.1B market value in 2014 with a predicted $21B by 2020 as reported by Wohlers 2015 [6]. This growth was possible due to AM technologies' ability to fabricate parts from a wide range of materials, making industries such as automotive, tooling, aerospace, or medical integrate them in their manufacturing processes [4,7].

Metals and metal alloys are commercially available for AM in powder form. They are mainly processed through powder bed fusion (PBF) techniques such as selective laser sintering (SLS),

selective laser melting (SLM) and direct energy deposition (DED) techniques such as electron beam melting (EBM) [3]. Tool steel, stainless steel, and aluminium (Al) alloys are the commonly used metal-based materials in AM. Mechanical properties are similar or, in some cases, better than the ones obtained through conventional manufacturing techniques [3]. Titanium (Ti), nickel (Ni) or cobalt (Co) based alloys have an excellent appeal for AM due to being difficult to manufacture through conventional techniques. Following extensive research done in this field, they are also commercially available [3]. The same motivation to ease manufacturing, remove tooling and increase the level of shape complexity for ceramic and composite materials such as cemented carbide through AM is present. Currently, the state of the art for these types of materials is situated just at a research level [8,9].

Tungsten carbide-cobalt (WC-Co) is the most common class of cemented carbides and a composite material that consists of hard carbide particles (WC) bonded together by a metallic binder phase (Co). It is a product of powder metallurgy (PM) and liquid-phase sintering (LPS), offering a unique combination of hardness, wear-resistance and toughness [10]. Additive manufacturing of WC-Co parts was first studied using PBF

1 TECHNICAL UNIVERSITY OF CLUJ-NAPOCA, DEPARTMENT OF MANUFACTURING ENGINEERING, 103-105, MUNCII AVENUE, 400641 CLUJ-NAPOCA, ROMANIA
2 GÜHRING ROMANIA, CONSTRUCTORILOR STREET 32, 407035 APAHIDA, ROMANIA
3 TECHNICAL UNIVERSITY OF CLUJ-NAPOCA, MATERIALS SCIENCE AND ENGINEERING DEPARTMENT, 103-105, MUNCII AVENUE, 400641 CLUJ-NAPOCA, ROMANIA

* Corresponding author: gadalean.rares.vasile@gmail.com

processes that use a laser as the thermal source, SLS and SLM. The aim is to melt the Co in the composition, enabling it to flow through the WC hard particles driven by the capillary forces, the liquid pressure and the viscosity, thus triggering the densification mechanism, liquid phase sintering [11].

Due to the short amount of time in which Co is in a molten state and the repeated heating and cooling cycles specific to PBF processes, LPS cannot complete all its phases. This results in parts with high porosity, low relative density and thermal cracks present in the structure [12,13]. Moreover, S. Kumar and A. Czekanskiet et al. [14] encountered the same limitations together with cobalt evaporation, even after optimising the process parameters and using a WC-Co powder with a relatively high amount of Co, 17wt%. The same impossibility in optimising process parameters is reported by E. Uhlmann et al. [15] with a direct incompatibility between obtaining a high part density using a high laser energy density and avoiding Co evaporation which requires a low laser energy density. These limitations affect the mechanical properties of the parts negatively. Solutions such as spherical WC-Co granules [16], a multi-pass scanning strategy [17], and the use of nanocomposite WC-Co powders [18] have been reported to improve some of the properties such as density, microhardness and thermal cracking, but still not enough when compared with WC-Co parts obtained through PM techniques.

Research using a two-step approach in AM of WC-Co has been intensified over the last years with the use of technologies such as binder jetting (BJ), thermoplastic 3D printing (T3DP) and 3D gel-printing (3DGP). These technologies have the same ability as PBF processes in producing complex-shaped parts. Still, they can only make a green body that requires further processing to be used as a functional part. This approach constitutes an advantage for manufacturing WC-Co because it involves a standard sinter-HIP cycle, allowing the LPS process to complete. A complete LPS process is crucial in achieving full density and a correct microstructure for WC-Co. Thus far, this could not be achieved by PBF processes [8,19,20]. Using this two-step approach, Ravi K. Enneti et al. fabricate WC-Co parts with microstructure, mechanical and magnetic properties that are comparable with WC-Co obtained through PM [21]. The reported density is close to 100% theoretical and is achieved with 12wt% Co. Similar microstructure and mechanical properties are reported for WC-Co parts through T3DP [22] and 3DGP [23]. In these cases, the reported density is 100% theoretical. These processes also have limitations. The complexity of the parts is relatively low, and only simple cuboid shapes are printed in the studies cited above, thus cancelling the advantages of AM [21-23]. Moreover, green parts fabricated through BJ are very fragile and require special measures to analyse and manipulate [24].

This work aims to fabricate WC-Co parts with a high degree of shape complexity and internal structures by employing SLS as the AM technology and sinter-HIP as the PM technology. The SLS process used is an indirect one. The WC-Co powder is mixed with a semi-crystalline polymer also in powder form. During the SLS process, only the polymer is laser sintered, thus assuring the structural integrity of the green bodies. The following subsequent debinding stage of the vacuum sintering process thermally removes it. This study takes further our research in this field of AM [1]. The purpose is to fabricate stable WC-Co green bodies through SLS using the most commonly used polymer, polyamide 12, [25], and improve the final part density by using high bulk density powders.

2. Experimental

Two WC-Co powders are used for this work, XP12 (WC-10Co) and AM WC701 (WC-12Co). They are both produced by the same company GTP, USA. Both are high bulk density powders with spherical particles, high flowability and a bulk density of 6.44 g/cm^3 for the XP12 and 6.26 g/cm^3 for the AM WC701, respectively. The semi-crystalline polymer used for the indirect SLS process is polyamide 12 (PA12) and is produced by ALM, Germany, under the commercial name PA650. It also has spherical particles and presents a good flowability, both requirements for a successful SLS process. Details of both powders are shown in TABLE 1.

TABLE 1

Properties of WC-Co and polymer powders used in the present study

Powder	D10 [μm]	D50 [μm]	D90 [μm]	Bulk density [g/cm^3]	Hall flow [s/50 g]
XP12	16	33	53	6.44	3
AM WC 701	18	25	35	6.26	9
PA650	30	55	100	0.46	—

A digital microscope Keyence VHX-6000 was used to reveal the powders' morphology at a magnification of 500×, Fig. 1. The stand out powder is the XP12, with near-perfect spherical particles that have a smoother surface when optically compared with the AM WC701 particles, thus explaining the increased flowability. Both WC-Co powders were homogenised with the PA12 powder by mechanical mixing. An industrial 3D mixer was used, and the total amount of mixing time for each composition was 4 h.

The total amount of PA12 that was mixed with each WC-Co powder is 10wt%. This value represented 60vol% and was determined in a previously published study [1] as the appropriate content for a successful indirect SLS process that produces WC-Co green bodies with good structural integrity and good geometry definition. Both powder compositions, XP12-PA12 and AM WC701-PA12 were optically analysed under the same digital microscope at the end of the mixing cycle, Fig. 2. A uniform distribution between WC-Co particles and the PA12 is observed, with the smaller WC-Co particles adhering to the bigger PA12 particles in both cases.

For the geometry of the green bodies, cubes with a side of 20 mm and cylinders with a diameter and height of 20 mm are chosen. These simple shape parts facilitate the dimensional measurements done after both SLS and sinter-HIP processes to determine density and shrinkage.
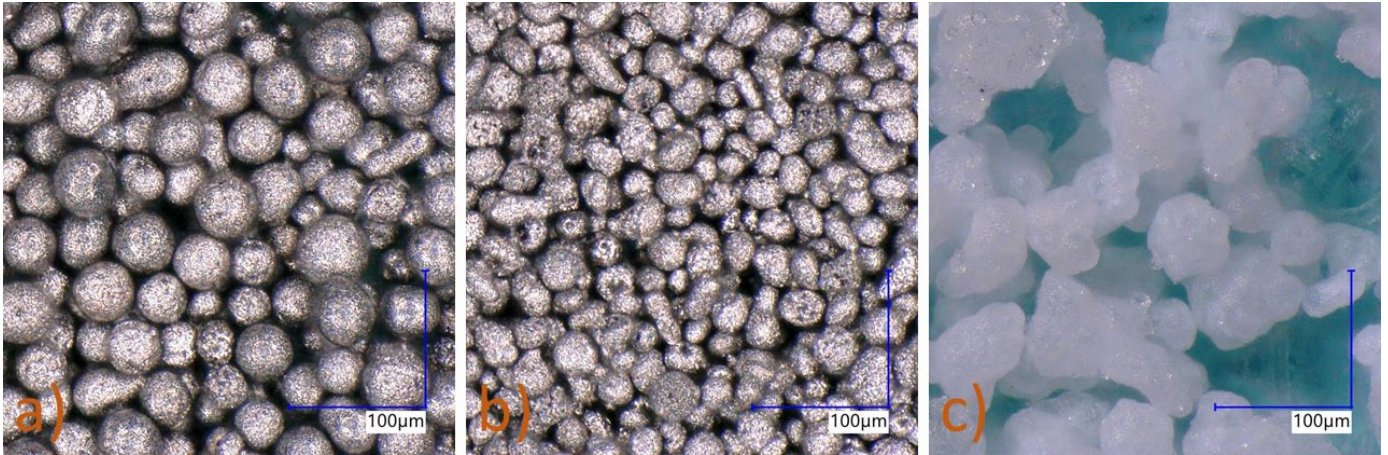
Fig. 1. Morphology of the used powders. XP12 (a), AM WC701 (b), PA650 (c)
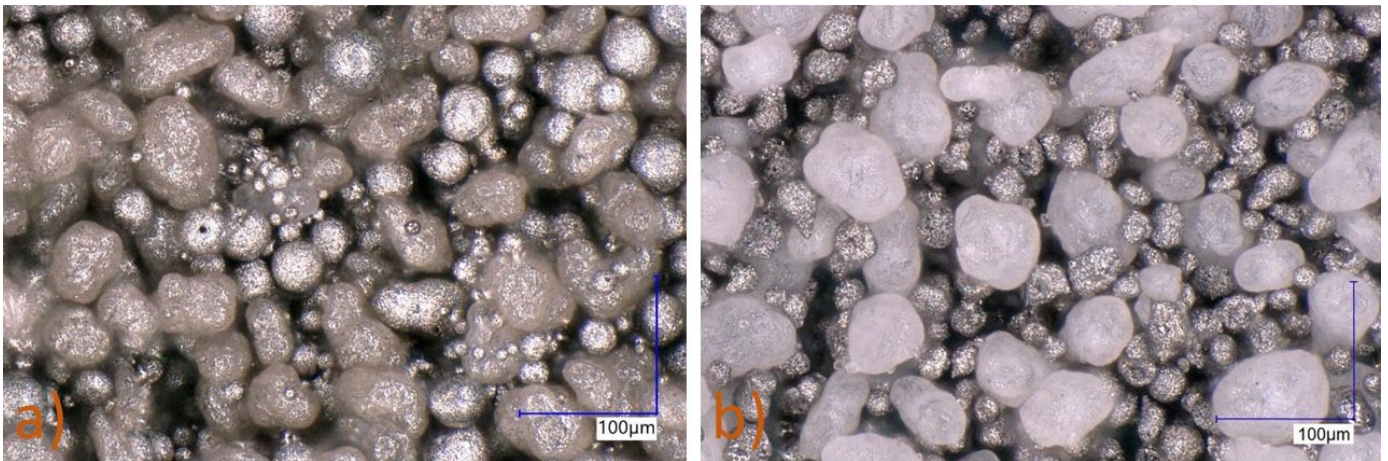

Fig. 2. Optical microscope image after the homogenisation cycle of XP12 (a) and AM WC701 (b)

An end mill with internal cooling channels was fabricated to study the indirect SLS process's capabilities to produce complex shape parts with internal structures. The details and dimensions are presented in Fig. 3.

All the green bodies from both powder compositions were fabricated using an SLS printer produced by the DTM Corporation, USA, under the commercial name, Sintersation 2000. It comes equipped with a modulated wave 50 W CO_2 laser system
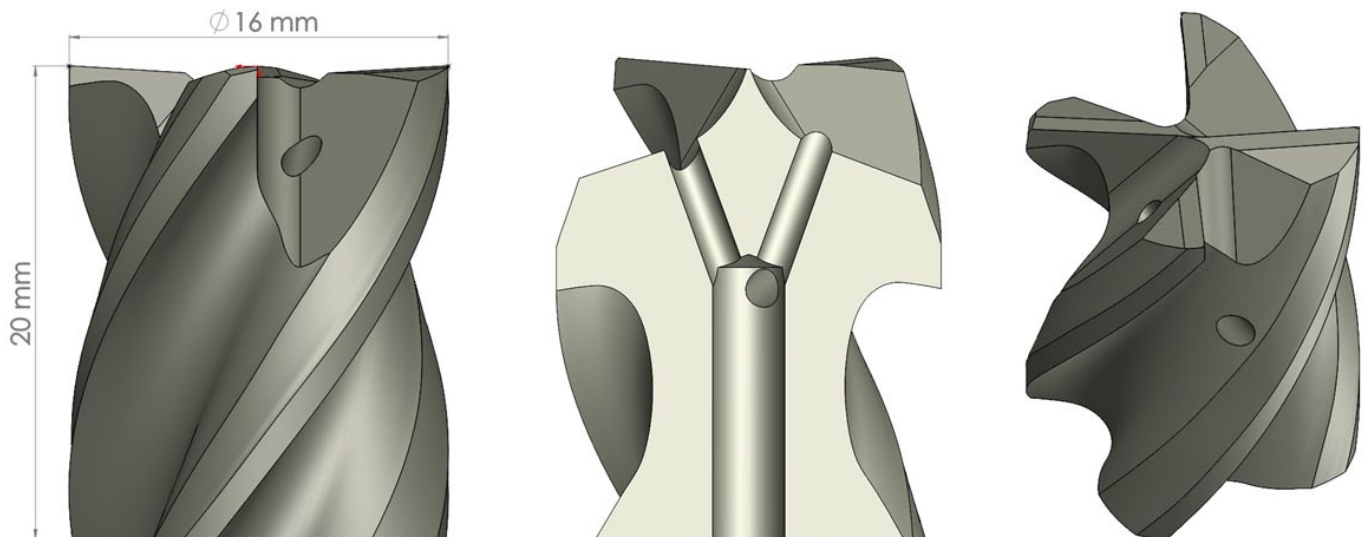

Fig. 3. Dimensions and CAD images of the SLS printed end mill

and a building chamber inerted with N_2 before starting the process to prevent oxidation [26]. As in any other AM process, the printing process begins with a 3D CAD model (.stl) sliced into equal thickness layers by a computer. A laser beam selectively scans each layer. This melts the polymer binder (PA12) and merges the particles, thus sintering the entire layer. At the end of this stage, the piston situated in the building chamber lowers its position with a value equal to a layer's thickness. Next, a counter rolling roller deposits a new layer of powder from one of the tanks and the laser sintering process starts again. The same stages are repeated until the entire height of the part is completed. A crucial SLS process parameter is the part bed temperature (T_b). The standard T_b value for any semi-crystalline polymer is set at 3-5°C below the initial melting point [27]. The T_b value for PA650 recommended by the producer is 170°C. For our study, this value was increased to 176°C, to avoid problems with parts being moved by the roller at the start of the process. The rest of the SLS process parameters are detailed in TABLE 2. One cubic green body from each composition was submerged in liquid nitrogen and fractured in half perpendicular to the printing plane to assess the SLS process's effectiveness. The cross-sections were analysed using the Keyence VHX-6000 digital microscope.

To sinter the green bodies into WC-Co parts, two separate cycles are used. First, a complete vacuum sintering cycle at 1400°C with a preliminary debinding stage at 800°C was performed in a PVA Tepla/Pfeiffer Balzers COV 733 R industrial furnace. The second cycle was completed in an ALD VKP 50/50/170 industrial sinter-HIP furnace starting with vacuum sintering at 1200°C followed by sinter-HIP at 1400°C with a pressure of 50 bar Ar. At the end of the HIP sintering cycle, the cubic and cylindric samples were measured to determine the shrinkage and density using the gravimetric method. Magnetic measurements were performed on all the samples using a Förster Koerzimat 1.097 HCJ equipment. A sample from each type of WC-Co powder (XP12 & AM WC701) was sectioned and polished to analyse the microstructure using a Sigma Zeiss scanning electron microscope (SEM) and also to measure the Vickers hardness (HV) using a Fischerscope HM2000 nanoindentation unit with an indentation force of 0.03 kgf. To assess the indirect SLS process's capabilities in fabricating complex shape parts, the end mill samples were scanned using optical 3D measurement equipment, Alicona InfiniteFocus G5. The samples are scanned in both states, as green bodies and also as sintered bodies. The resulted scans are overlaid with the original 3D model and compared using the software provided by Alicona.

3. Results and discussions

The approach used in this work is an industrial one, utilising commercially available raw materials and 3D printing equipment. This leads to a few challenges that needed to be overcome to fabricate the WC-Co green bodies successfully. First, the powder tanks of the Sinterstation 2000 were divided into four compartments to allow the usage of a smaller volume

TABLE 2

SLS process parameters

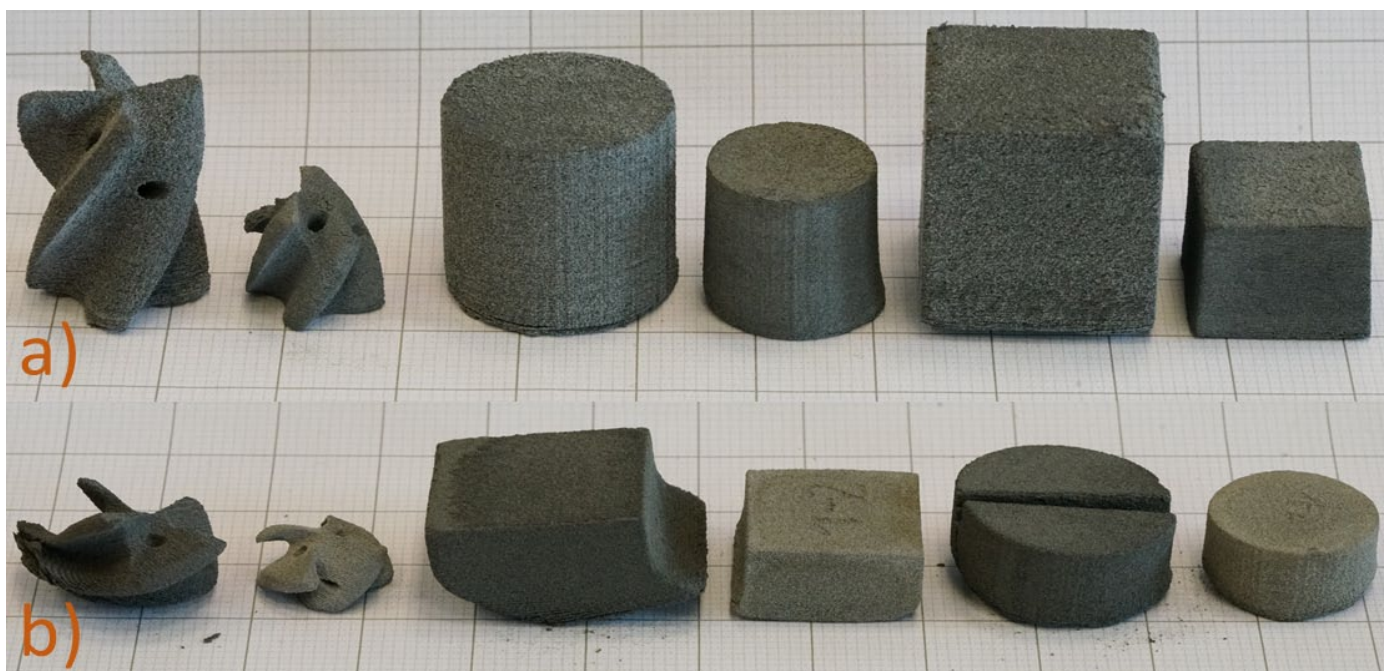| Laser Power [W]	4.5
Layer Thickness [mm]	0.10
Scan Spacing [mm]	0.15
Scan Speed [mm/s]	1257
Laser Energy Density [J/mm²]	0.239
Roller speed [mm/s]	80
Part Bed Temperature [°C]	176

Fig. 4. Green and sintered samples. AM WC701 (a) and XP12 (b)

of powder, 4 l, instead of the normal volume, 30 l, for the SLS machine to function. A big compartment at the bottom of the tank containing ballast powder is first created. On top of it sit the remaining three compartments separated from the bottom one with an aluminium foil. The top compartments are separated between each other using two thin plastic separators placed in the tank before the powder is poured in and removed after each compartment has the same powder height. The middle compartment contains the WC-Co/PA12 powder mixture, with each side compartment containing the same ballast powder. The second challenge was to avoid the samples' dislocation from the powder bed by the powder spreading roller. This was encountered with the first tested powder composition, XP12-PA12, after just a few built layers.

Several changes to the process parameters were made to solve this unwanted phenomenon, leading to stopping the entire process. The total number of samples been built was reduced thus, increasing the gaps between samples. The powder spreading roller's speed was reduced to its minimum value, 80 mm/s, and the Tb increased to 176°C. These changes make the completion of the indirect SLS process successful. Due to a large amount of powder used with all the process restarts required after each parameter change, the samples from the XP12-PA12 composition needed to be scaled down thus, achieving only 10mm in height instead of the original 20mm. This also explains the deformed end mill samples from the same powder composition presented in Fig. 4. For the AM WC701-PA12 composition, the printing process went smoother, resulting in green bodies with an excellent geometrical definition, see Fig. 4. Dimensional accuracy of ±2% for the cubic and cylindric samples was achieved. Moreover, in both cases, the samples present good structural integrity; they are easy to manipulate and were not affected by the brushing operation necessary to remove them from the powder bed.

The exact good geometrical definition and dimensional accuracy are revealed by the 3D scan overlay of the green end mill

sample fabricated using the AM WC701-PA12 composition, see Fig. 5. In the green state, the end mill sample presents a dimensional deviation between 0.2-0.6 mm for most of the scanned area, translating to a dimensional accuracy between 1-3%. The maximum deviation of 1.2 mm is present just at the bottom of the sample and is present due to the samples' movement in the powder bed. This movement is induced by the powder spreading roller at the beginning of the printing process and could not be entirely avoided even after changing the above-mentioned process parameters.

The 3D scan overlay of the sintered end mill sample is also represented in Fig. 5. In this case, the majority of the dimensional deviation is situated between 0.2-1 mm. These values are similar to those obtained for the green end mill sample, suggesting a uniform shrinkage during sintering. Despite this, two of the four cutting edges of the scanned end mill have broken off during the furnace sintering process. This problem occurs for all the end mill samples fabricated using the AM WC701-PA12 composition, with some of them collapsing almost entirely.

Moreover, due to the friction between the samples and the support plate during furnace sintering, the shrinkage at the bottom of the end mill sample is reduced; thus, creating a deformed area. This is confirmed by the 3D scan overlay having a dimensional deviation value of 2.8 mm. This known as the "elephant foot" phenomenon [28], is also visible in Fig. 4 for the cubic and cylindric samples. The same problem is not visible on the sintered XP12-PA12 samples.

Analysing the fractured cross-sections made on the cubic green bodies for both powder compositions, it is observed that the laser sintering process of the polymer binder has not worked as expected in each case. This is highlighted by the presence of the unmelted PA12 particles, see Fig. 6. This problem was not encountered during our previous published work [1], where the same laser parameters were used to fabricate green bodies from a mixture containing a ready to press WC-Co powder and the same polymer binder, PA12. This means that both high bulk
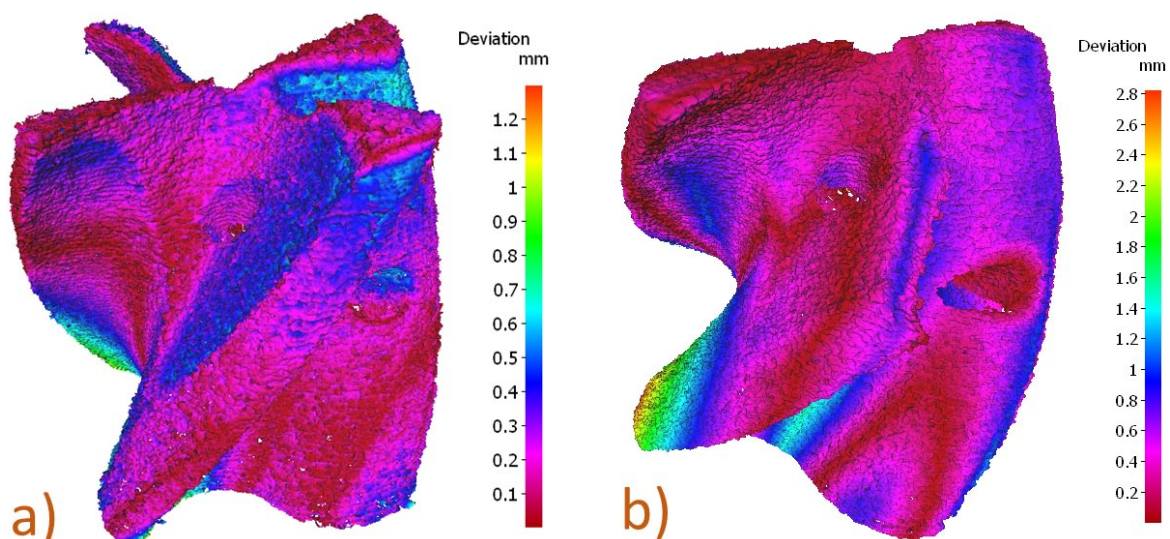

Fig. 5. The 3D scan overlays of the AM WC701 end mill samples. The original 3D model (.stl) is compared with the green body (a) and with the sintered sample (b)
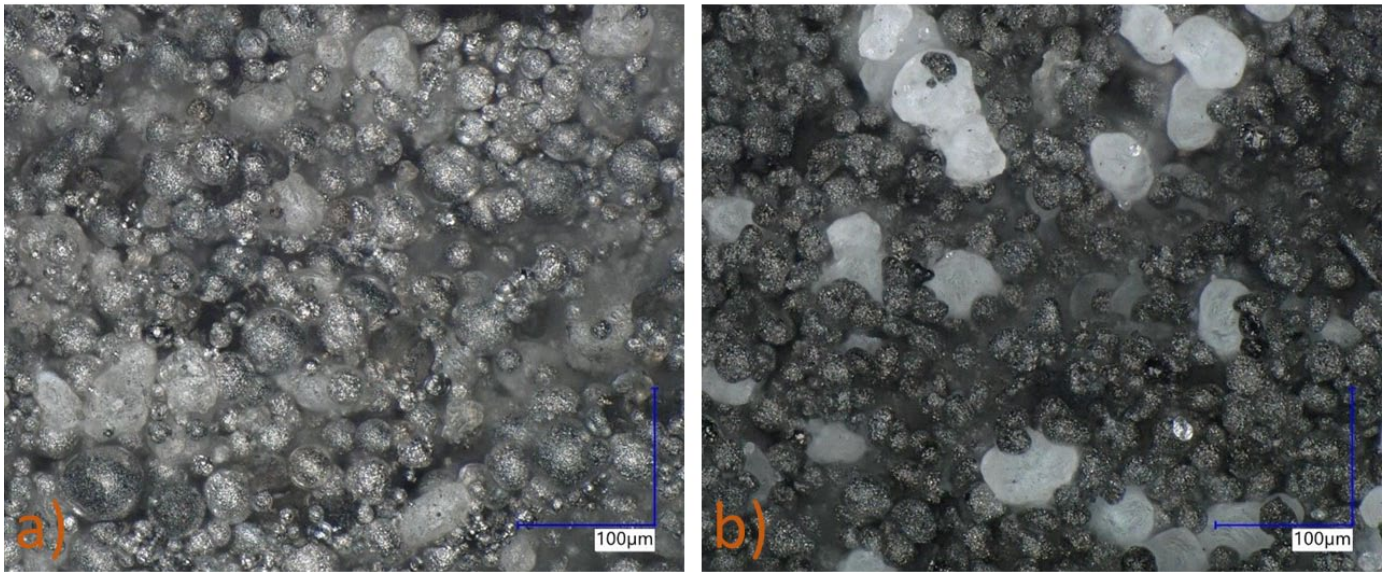
Fig. 6. Fracture cross-sections of the cubic green bodies. XP12 (a) and AM WC701 (b)

density powders used in this work, XP12 and AM WC701, decreased the sintering ability of PA12 during the SLS process. This incomplete sintering of the polymer binder explains the problems encountered at the beginning of the process, with parts being dislocated in the roller's powder bed. This is due to the weak bond created between the powder bed and the first scanned layer. This weak bond between the PA12 particles is present throughout the green body, layer by layer, leading to low overall strength. During the debinding phase of the vacuum sintering cycle, the end mill green samples are affected the most by this low strength; thus, causing parts of them to break off or even collapse entirely.

The average green density obtained for the XP12-PA12 composition is 3.76 g/cm^3, and for the AM WC701-PA12 composition is 4.40 g/cm^3. These density values represent 26% and 31% of the theoretical density, see Fig. 7. This translates to an improvement of 64% for XP12 and 91% for AM WC701 when comparing the average green density values with the ones ob-

tained in our previous work [1]. This considerable improvement in green density is explained by the increased bulk density of both WC-Co powders used in this work. In both cases, the bulk density is increased more than two times compared to the bulk density of the ready to press WC-Co powder used in [1]. Due to no pressure being applied by the roller during layer generation, the resulting green bodies inherit the density of the powder bed. Successful furnace sintering of WC-Co is dependent on the initial density of the green bodies; thus, confirming the importance of using high bulk density powders.

Although the minimum 50% of theoretical density recommended in the PM industry for the green bodies to achieve full densification after furnace sintering was not achieved, for the AM WC701 powder, the average density following the sinter-HIP cycle is 11.72 g/cm^3. This represents 82% theoretical density and offers a 24% improvement over the average sintered density reported in reference [1] using the same amount of 60 vol% PA12 for a similar WC-Co powder with 12 wt% Co. A shrink-
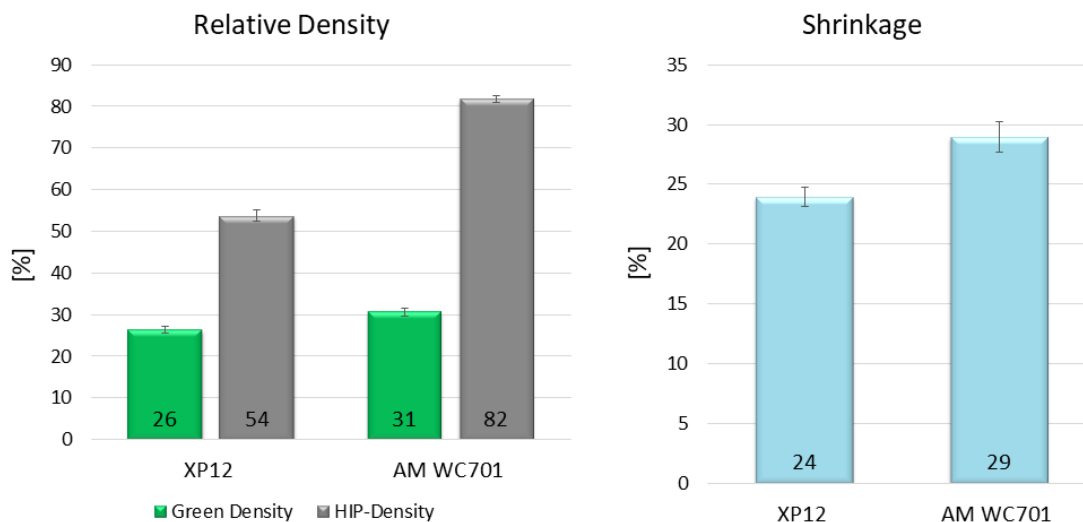

Fig. 7. Relative geometrical density and shrinkage for each type of WC-CO powder

age value of 29% (Fig. 7) is in line with what is achieved with binder jetting by [21] and is significantly smaller than the value of 43% achieved for shrinkage in reference [1].

The furnace sintering process of the green bodies fabricated using the XP12 powder did not work as expected. The average density obtained after the sinter-HIP cycle is 7.80 g/cm^3 and represents only 54% of the theoretical density. It even fails in matching the average density of 66% theoretical achieved with a ready to press WC-Co powder in our previous work [1]. The poor densification of the XP12-PA12 composition is confirmed when analysing the polished samples using a scanning electron microscope, see Fig. 8. At a lower magnification of 100×, the entire structure is dominated by porosity.

Moreover, the WC-Co particles are visible, and most of them have maintained their original spherical shape. At larger magnification, 2000×, it can be observed that the previously observed porosity is limiting the formation of sintering necks between WC-Co particles, and it appears that the proper LPS has only taken place locally. For the XP12-PA12 samples, the microstructural investigation indicates that the current sintering parameters are insufficient for such materials.

On the other hand, a similar SEM analysis on the polished AM WC701 sample (Fig. 9) revealed a microstructure comprised of medium-sized WC grains, averaging between 1.5-2.5 μm in size embedded in a well-distributed Co matrix. It is worth mentioning that regardless of the used magnification, in this case also, both macro and micropores are observed together with areas containing a high amount of Co. These pores originate from the debinding stage of the green bodies, when the polymer evaporates entirely, leaving behind a large amount of residual porosity. To achieve full densification of the samples, Co must fill up the porosity during the liquid phase sintering. The densification is dependent on the amount of Co present in the composition and good contact between particles. By employing a high bulk density powder, the contact between WC-Co particles has been improved compared to the ready to press powder used in [1] because, at the same amount of Co (12wt%), a 24% increase in the final density was achieved.

Nevertheless, only improving the contact between particles was not enough to achieve total density. For future work, an approach using a high bulk density powder together with a high amount of Co in the range of 17-20 wt% may lead to
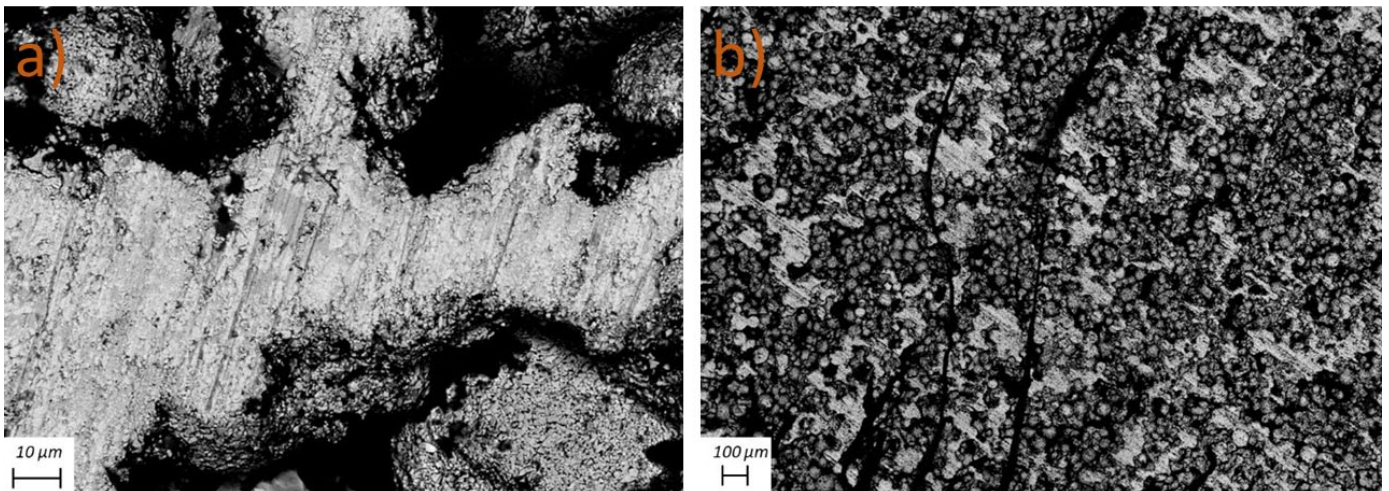

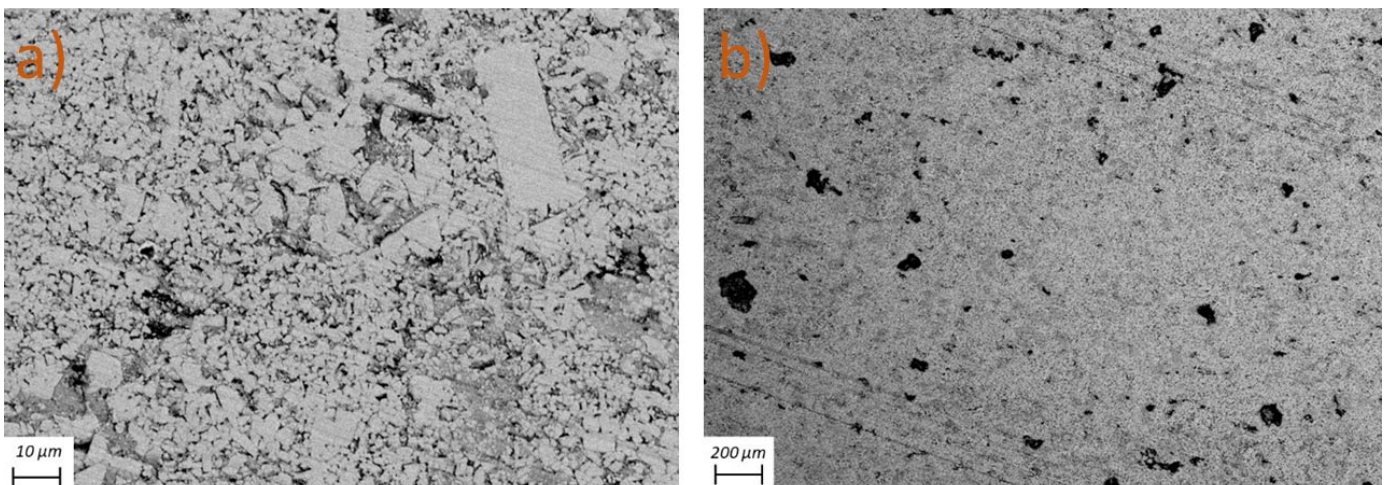Fig. 8. SEM images of cross-sectioned XP12 sample. Magnification 2000× (a) and 100× (b)

Fig. 9. SEM images of cross-sectioned AM WC701 sample. Magnification 2000× (a) and 100× (b)

Magnetic Properties
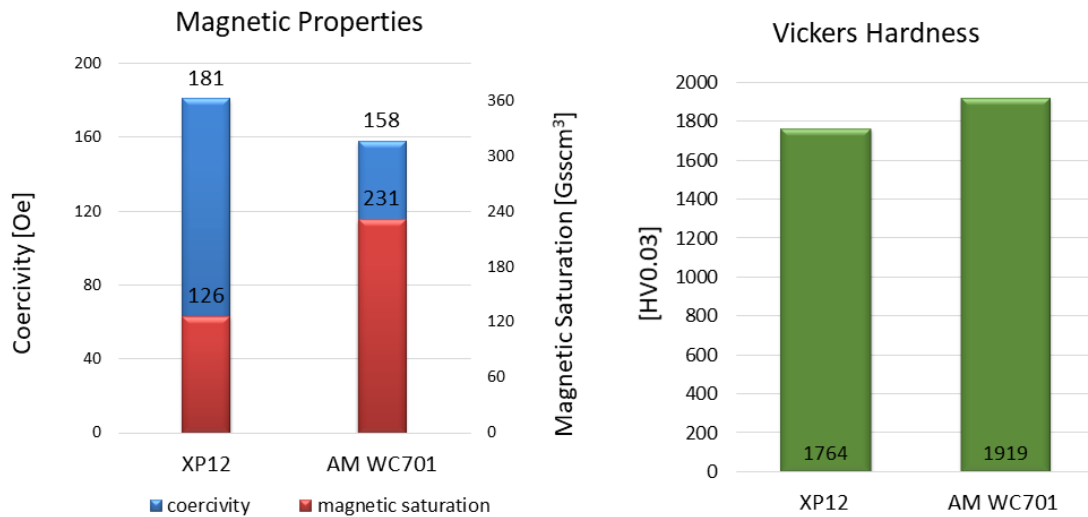

Vickers Hardness

Fig. 10. Magnetic properties and hardness for each type of WC-Co powder

full densification by favouring the rearrangement mechanism responsible for the most densification that takes part during liquid phase sintering. The poor densification of the XP12 samples cannot only be attributed to the reduced amount of Co, 10 wt%. The powder's quality also influences the final obtained density.

For cemented carbide, the resulting hardness after furnace sintering depends on the wt% of Co and the WC grains' mean size. In the case of the XP12 samples, the microhardness measurements were challenging to make due to the high degree of porosity. Nevertheless, three measurements were taken, resulting in an average value of 1764 HV0.03 and are presented in Fig. 10. The exact number of hardness measurements are made for the AM WC701 sample resulting in an average value of 1919 HV0.03 (Fig. 10). Both WC-Co powders present high hardness values for a cemented carbide with medium-sized WC grains (1.5-2.5 µm) and a Co content of 12 wt% (AM WC701) and 10 wt% (XP12) respectively. The obtained microhardness values are in good relation with the observed microstructuress.

Fig. 10 also presents the magnetic properties of the tested WC-Co powders. A magnetic saturation value of 231 Gss·cm^3 for the AM WC701 powder could indicate free carbon in the sintered samples. The obtained value is larger than the producer's maximum value at full carbon saturation, of 154 Gss·cm^3. However, this can be assigned to a certain amount of Co alloying with excess carbon, originating from the decomposition of PA12, and thus, the material is behaving such as ferrite. Similar behaviour has been previously reported [29]. The average free ferromagnetic Co for the AM WC701 samples is 11.5% suggesting that no reaction during sintering occurred, leading to different compounds. In the case of XP12 samples, the low magnetic saturation of 126 Gss·cm^3 corroborated with the low amount of free ferromagnetic Co, 6.3%, further highlighting the failed furnace sintering process.

4. Conclusions

With the use of high bulk density powders, this research aimed to take further our published work in reference [1] and improve upon the density of 3D printed WC-Co parts. This was achieved in the case of the AM WC701-PA12 powder composition with cubic and cylindric samples having an average density of 11.72 g/cm^3, representing 82% of the theoretical density. This average density was achieved at the end of the sinter-HIP process and translated to a 24% improvement over the highest density achieved in our previous work [1] using a WC-Co powder with the same Co, 12 wt%. The second type of high bulk density powder used in this work, XP12, has not undergone a successful sintering process resulting in samples with a density of 7.80 g/cm^3, representing only 54% of the theoretical density. Stable and easy to manipulate green bodies were fabricated through the indirect SLS process using both powder compositions, AM WC701-PA12 and XP12-PA12. Moreover, in the case of the AM WC701-PA12 composition where the SLS process worked as expected the 3D scan overlays reveal a dimensional accuracy of 1-3% for the green end mill sample that only slightly increases to 5% for the sintered end mill sample. These results have shown that the approach used in this study has the right capabilities in fabricating accurate WC-Co parts together with a high degree of shape complexity. The challenges faced throughout this work such as green bodies dislocated in the powder bed, end mill samples partially breaking off during the sintering process and also not achieving full density leave room for future research. Increasing the laser energy density during the indirect SLS process and using a WC-Co powder with a higher Co content (17-20 wt%) could lead to better results regarding the problems mentioned above.

Acknowledgement

REFERENCES

[1] O.D. Jucan, R. Gădălean, H.F. Chicinaş, M. Hering, N. Bâlc, C.O. Popa, Int. J. Refract. Met. Hard Mater. 105498 (2021).

[2] A. Gebhardt, J.S. Hötter, Additive Manufacturing: 3D Printing for Prototyping and Manufacturing, Carl Hanser Verlag GmbH & Company KG, 2016.

[3] T.D. Ngo, A. Kashani, G. Imbalzano, K.T.Q. Nguyen, D. Hui, Compos. Part B Eng. **143** 172-196 (2018).

[4] R. Singh, A. Gupta, O. Tripathi, S. Srivastava, B. Singh, A. Awasthi, S.K. Rajput, P. Sonia, P. Singhal, K.K. Saxena, Mater. Today Proc. **26**, 3058-3070 (2020).

[5] M. Jiménez, L. Romero, I.A. Domínguez, M. del M. Espinosa, M. Domínguez, Complexity 2019 (2019).

[6] B. Post, R.F. Lind, P.D. Lloyd, V. Kunc, J.M. Linhal, L.J. Love, in: Proc. Solid Free. Fabr. Symp. Addit. Manuf. Conf. Austin, TX, USA, pp. 8-10, 2016,

[7] K. Rajaguru, T. Karthikeyan, V. Vijayan, Mater. Today Proc. **21**, 628-633 (2020).

[8] A. Aramian, S.M.J. Razavi, Z. Sadeghian, F. Berto, Addit. Manuf. **33**, 101130 (2020).

[9] T. Moritz, S. Maleksaeedi, in: Addit. Manuf., Elsevier, pp. 105-161 (2018).

[10] V. Sarin, Comprehensive Hard Materials, Newnes, 2014.

[11] N.B. Dahotre, S. Harimkar, Laser Fabrication and Machining of Materials, Springer Science & Business Media, 2008.

[12] X.C. Wang, T. Laoui, J. Bonse, J.-P. Kruth, B. Lauwers, L. Froyen, Int. J. Adv. Manuf. Technol. **19**, 351-357 (2002).

[13] S. Kumar, J. Mater. Process. Technol. **209**, 3840-3848 (2009). DOI: https://doi.org/10.1016/j.jmatprotec.2008.08.037

[14] S. Kumar, A. Czekanski, Rapid Prototyp. J. **23**, 1202-1211 (2017).

[15] E. Uhlmann, A. Bergmann, W. Gridin, Procedia CIRP **35**, 8-15 (2015).

[16] J. Chen, M. Huang, Z.Z. Fang, M. Koopman, W. Liu, X. Deng, Z. Zhao, S. Chen, S. Wu, J. Liu, W. Qi, Z. Wang, Int. J. Refract. Met. Hard Mater. **84**, 104980 (2019). DOI: https://doi.org/10.1016/j.ijrmhm.2019.104980

[17] A. Fortunato, G. Valli, E. Liverani, A. Ascari, Lasers Manuf. Mater. Process. **6**, 247-262 (2019)

[18] A. Domashenkov, A. Borbély, I. Smurov, Mater. Manuf. Process. **32**, 93-100 (2017). DOI: https://doi.org/10.1080/10426914.2016.1176195

[19] M. Padmakumar, Lasers Manuf. Mater. Process. **7**, 338-371 (2020).

[20] Y. Yang, C. Zhang, D. Wang, L. Nie, D. Wellmann, Y. Tian, Int. J. Adv. Manuf. Technol. **108**, 1653-1673 (2020).

[21] R.K. Enneti, K.C. Prough, T.A. Wolfe, A. Klein, N. Studley, J.L. Trasorras, Int. J. Refract. Met. Hard Mater. **71**, 28-35 (2018).

[22] I. Fraunhofer, J. Ceram. Sci. Technol. **8**, 155-160 (2016).

[23] X. Zhang, Z. Guo, C. Chen, W. Yang, Int. J. Refract. Met. Hard Mater. **70**, 215-223 (2018).

[24] C.L. Cramer, P. Nandwana, R.A. Lowden, A.M. Elliott, Addit. Manuf. **28**, 333-343 (2019).

[25] S.D. Nath, S. Nilufar, Polymers (Basel). **12**, 2719 (2020).

[26] N.P. Juster, Assem. Autom. **14**, 14-17 (1994).

[27] M. Schmid, K. Wegener, Procedia Eng. **149**, 457-464 (2016).

[28] R. Raman, R.M. German, Metall. Mater. Trans. A **26**, 653-659 (1995).

[29] H.F. Chicinaş, T.F. Marinca, P. Götze, A. Eckert, C.O. Popa, J. Mater. Sci. **53**, 2901-2910 (2018).